



MIT Open Access Articles

Stratospheric Ozone in the Last Glacial Maximum

The MIT Faculty has made this article openly available. **Please share** how this access benefits you. Your story matters.

As Published	10.1029/2020JD032929
Publisher	American Geophysical Union (AGU)
Version	Final published version
Citable link	https://hdl.handle.net/1721.1/133948
Terms of Use	Creative Commons Attribution 4.0 International license
Detailed Terms	https://creativecommons.org/licenses/by/4.0/

JGR Atmospheres



RESEARCH ARTICLE

10.1029/2020JD032929

Key Points:

- Modeled ozone in Last Glacial Maximum is increased in tropical lower stratosphere but decreased in most other regions compared to preindustrial
- Combined changes in stratospheric and tropospheric ozone lead to a decrease in total ozone column over the globe except in a few regions
- Surface ultraviolet radiation is increased in the Northern Hemisphere extratropics, especially over the Laurentide ice caps, and near 60°S

Correspondence to:

M. Wang,
wmingch@uw.edu

Citation:

Wang, M., Fu, Q., Solomon, S., White, R. H., & Alexander, B. (2020). Stratospheric ozone in the Last Glacial Maximum. *Journal of Geophysical Research: Atmospheres*, 125, e2020JD032929. <https://doi.org/10.1029/2020JD032929>

Received 15 APR 2020

Accepted 17 SEP 2020

Accepted article online 20 OCT 2020

Stratospheric Ozone in the Last Glacial Maximum

Mingcheng Wang¹ , Qiang Fu¹ , Susan Solomon² , Rachel H. White³ , and Becky Alexander¹ 

¹Department of Atmospheric Sciences, University of Washington, Seattle, WA, USA, ²Department of Earth, Atmospheric, and Planetary Sciences, Massachusetts Institute of Technology, Boston, MA, USA, ³Barcelona Supercomputing Center, Barcelona, Spain

Abstract Using the Whole Atmosphere Community Climate Model version 6, stratospheric ozone in the Last Glacial Maximum (LGM) is investigated. It is shown that, compared with preindustrial (PI) times, LGM modeled stratospheric temperatures are increased by up to 8 K, leading to faster ozone destruction rates for gas phase reactions, especially via the Chapman mechanism. On the other hand, stratospheric hydroxyl radical (OH) and nitrogen oxides (NO_x) concentrations are decreased by 10–20%, which decreases catalytic ozone destruction, thereby decreasing ozone loss rates. The net effect of these two compensating mechanisms in the upper stratosphere (above 15 hPa) is a vertically integrated 1–3 Dobson unit (DU) decrease during the LGM. In the lower stratosphere (tropopause to 15 hPa), changes in the stratospheric overturning circulation and resulting transport dominate changes in ozone. Consistent with a weakening of the residual circulation in the LGM, lower stratospheric ozone is increased by 2–5 DU in the tropics and decreased by 5–10 DU in the extratropics, but the latter is partly compensated by ozone increases due to a lower tropopause. It is found that tropospheric ozone is decreased by about 5 DU in the LGM versus PI. Combined changes in stratospheric and tropospheric ozone lead to a decrease in total ozone column everywhere except over the northeast North America, equatorial Indian and West Pacific Oceans. Surface ultraviolet radiation in the LGM versus PI is increased over the Northern Hemisphere middle and high latitudes, especially over the ice caps, and over the Southern Hemisphere near 60°S.

1. Introduction

As a key component of the Earth system, stratospheric ozone protects life on Earth from hazardous ultraviolet (UV) radiation, and has a crucial impact on the tropospheric chemistry. Rohrer and Berresheim (2006) showed that tropospheric hydroxyl radical (OH) is linearly correlated with UV radiation based on 5 years of measurements in Germany. Murray et al. (2014) found that stratospheric ozone, via its impact on surface UV radiation, is an important factor controlling variability in tropospheric OH over glacial-interglacial periods in a chemistry-climate model. In addition, stratospheric ozone could impact tropospheric climate (e.g., Chiodo & Polvani, 2017; Noda et al., 2017; Nowack et al., 2015; Szopa et al., 2019). Szopa et al. (2019) found that modeled global surface temperature in the Eocene differed by as much as 14%, depending on whether the stratospheric ozone column abundance was consistently calculated or prescribed at preindustrial (PI) levels.

During the Last Glacial Maximum (LGM), the stratosphere, including stratospheric ozone, is expected to be different from the PI climate because of lower greenhouse gas concentrations (e.g., CO₂, CH₄, and N₂O), widespread ice sheets (up to 3–4 km thick) in the Northern Hemisphere (NH) and lower sea surface temperatures (SSTs). Compared to the rich literature on stratospheric ozone for the current and future climates, there are only a few studies on stratospheric ozone in the LGM (Crutzen & Brühl, 1993; Martinerie et al., 1995; Murray et al., 2014; Noda et al., 2018; Rind et al., 2009). From a lack of better knowledge, past model simulations of the glacial climate have often assumed that stratospheric ozone is similar to the PI climate (e.g., Kaplan et al., 2006; Levine et al., 2011; Valdes et al., 2005). However, as indicated above, there are multiple reasons to expect ozone in the LGM to be different to the PI distribution, and this study provides an analysis of these differences using a state-of-the-art chemistry climate model.

Pioneering research about stratospheric ozone in the LGM was carried out by Crutzen and Brühl (1993), who used a “one and a half” dimensional (1^{1/2}-D) model. Martinerie et al. (1995) utilized a two-dimensional (2-D) model to further investigate the chemical composition of the atmosphere during

©2020. The Authors.

This is an open access article under the terms of the Creative Commons Attribution License, which permits use, distribution and reproduction in any medium, provided the original work is properly cited.

the LGM. Both of these studies found only small changes in stratospheric ozone between the LGM and the PI climate, despite large changes in atmospheric greenhouse concentrations. Rind et al. (2009) examined stratospheric ozone in the LGM using the 3-D GISS Global Climate Middle Atmosphere model ($4^\circ \times 5^\circ$ and 53 layers) with linearized ozone chemistry (McLinden et al., 2000). The model used in Rind et al. (2009) did not consider stratospheric heterogeneous chemical processes nor tropospheric chemistry but instead simulated tropospheric ozone using a simple relaxation approach. Rind et al. (2009) found that reduced nitrogen oxides (NO_x) and chlorine in the LGM lead to increases in stratospheric ozone, and much higher ozone concentrations in the polar, lower stratosphere associated with an intensified Brewer-Dobson circulation (BDC) in the lowermost stratosphere, which in turn leads to stronger stratosphere-to-troposphere transport of ozone.

Recent ice core observations of a proxy for tropospheric oxidants suggested that tropospheric ozone concentrations may have been higher in cold climates compared to warm climates (Geng et al., 2017), the opposite of expectations based on changes in temperature-dependent surface emissions of ozone precursor gases. Geng et al. (2017) hypothesized that higher tropospheric ozone in the extratropics could be due to increased transport of stratospheric ozone to the surface driven by an enhanced BDC in the glacial climate (Rind et al., 2001, 2009). An alternative hypothesis was that reactive halogen chemistry could be enhanced in the glacial climate, with potential implications for tropospheric ozone abundances (Geng et al., 2017). Using the Whole Atmosphere Community Climate Model version 6 (WACCM6), Fu et al. (2020) showed that the BDC during the LGM is consistently slower than modern climate. By transporting stratospheric ozone from the tropics, where it is produced, to the poles, the BDC plays a substantial role in determining the spatial distribution of ozone and thus surface UV radiation. This study analyzes the changes in ozone and UV radiation in the LGM including those resulting from changes in BDC, as simulated by WACCM6 (Fu et al., 2020).

This paper consists of four sections. Section 2 provides a brief description of WACCM6 and the model simulations. Section 3 presents the main results, and section 4 summarizes and concludes the paper.

2. Model Description and Simulations

2.1. Model Description

The WACCM6 is the high-top atmospheric component of the National Center for Atmospheric Research (NCAR) Community Earth System Model 2 (Gettelman et al., 2019), with a horizontal resolution of 1.25° longitude by 0.9° latitude with 70 vertical levels extending from the surface to 6×10^{-6} hPa (~ 140 km). In WACCM6, stratospheric heterogeneous chemical processes are parameterized following Wegner et al. (2013) and Solomon et al. (2015). Chemical kinetics and photochemical rate constants have been updated following Jet Propulsion Laboratory (JPL) 2015 recommendations (Burkholder et al., 2015). The updated tropospheric chemistry scheme in WACCM6 leads to an improvement to the isoprene oxidation as well as other ozone precursors and thus the tropospheric ozone simulation, as compared to the observations (Emmons et al., 2020). WACCM6 was run by specifying SST and sea ice. We coupled the WACCM6 model with the CLM4.0 land model (Oleson et al., 2010) and utilized the CLM4.0 LGM lower boundary conditions from the CESM Paleo Working group (e.g., Brady et al., 2013). In the LGM simulations, the plant functional type distribution is fixed under PI conditions, but the leaf area index, vegetation height, and biogenic emissions are estimated as a function of the changed climate (Guenther et al., 2012; Thornton et al., 2007).

WACCM6 is able to reproduce variability in the middle atmosphere as derived from reanalyses (e.g., MERRA and ERA-Interim), including the frequency of stratospheric sudden warmings (Gettelman et al., 2019) and BDC (Fu et al., 2020). WACCM6 has an internally generated quasi-biennial oscillation in the lower stratosphere (Garcia & Richter, 2019; Gettelman et al., 2019). The WACCM model suite has a realistic evolution of the Southern Hemisphere (SH) springtime ozone hole over the latter half of the twentieth century (Solomon et al., 2015). For more details, the readers are referred to Gettelman et al. (2019).

2.2. Model Simulations

Table 1 describes the simulations carried out for the study: (1) LGM simulation with prescribed SSTs derived from models ($\text{LGM}_{\text{PMIP3}}$), (2) LGM simulation with SSTs based on proxy data ($\text{LGM}_{\text{PROXY}}$), and (3) PI climate simulation. With the first 10 years discarded for spin-up, the results presented here are based on the

Table 1

Model Simulations

Simulation names		LGM _{PMIP3}	LGM _{PROXY}	PI
CO ₂		185 ppm	185 ppm	284 ppm
CH ₄		349 ppb	349 ppb	810 ppb
N ₂ O		200 ppb	200 ppb	273 ppb
ODS		0	0	0
CO	Fires	0.1 × Preind.	0.1 × Preind.	Year 1850
	Ocean	Preind.	Preind.	Year 1850
	Fuel Combustion	0	0	Year 1850
NO _x	Lighting	Interactive	Interactive	Interactive
	Fires	0.1 × Preind.	0.1 × Preind.	Year 1850
	Soil	0.98 × Preind.	0.98 × Preind.	Year 1850
	Fuel Combustion	0	0	Year 1850
SSTs		PMIP3 ^a multimodel mean	MARGO proxy data	1870–1890 average
Sea ice		PMIP3 multimodel mean	PMIP3 multimodel mean	1870–1890 average
Ice sheet topography		Abe-Ouchi et al. (2015)	Abe-Ouchi et al. (2015)	Modern climate
Orbital forcing		21,000 years ago	21,000 years ago	Year 1850

^aPMIP3 is Paleoclimate Modeling Intercomparison Project Phase 3.

simulations from Years 11 to 30; sensitivity studies extending simulations to 60 years find that using Years 11–30 provides robust results for the analysis presented here.

The concentrations of CO₂, CH₄, and N₂O for the LGM (PI) are 185 (284) ppm, 349 (810) ppb, and 200 (273) ppb, respectively. The surface concentrations of long-lived atmospheric species represent the Year 1850 for the PI, and all anthropogenic emissions are turned off in the LGM. The orbital parameters are conditions 21,000 years ago for LGM simulations and Year 1850 for the PI simulation. For the PI simulation, the SSTs/sea ice are the climatological averages of the Year 1870–1890 based on observations (Rayner et al., 2003) with a seasonal cycle. For LGM_{PMIP3}, we used the PMIP3 multimodel mean SST/sea ice for seven models that had both LGM and historical runs (Braconnot et al., 2012). The SSTs and sea ice for the LGM were then obtained as the model differences between the LGM and modern climate simulations plus corresponding observed SSTs/sea ice in modern climate (Fu et al., 2020). For LGM_{PROXY}, the LGM-PI SST differences are taken from the MARGO proxy data (Kucera et al., 2005), while sea ice is the same as in LGM_{PMIP3}. The LGM ice sheet topography was from Abe-Ouchi et al. (2015).

For ozone-depleting substances, WACCM6 considers 17 organic halogens, among which 4 (i.e., methyl bromide, methyl chloride, dibromomethane, and bromoform) include natural sources. Therefore, we set these 4 surface mixing ratios in the LGM to PI levels, while the remaining 13 species are not included in the LGM and PI simulations. Emissions of CO and NO_x in the LGM were scaled with PI emissions (Table 1) following Murray et al. (2014). The CO emissions from fires, ocean, and fuel combustion in the LGM were scaled to 0.1, 1, and 0 of the PI levels, while the NO_x emissions from fires, soil, and fuel combustion in the LGM were scaled to 0.1, 0.98, and 0 of the PI values. The emission of NO_x from lightning is simulated with the parameterization of Price and Rind (1992).

3. Results

3.1. Temperature Changes

Figure 1 shows the annual and zonal mean temperature change for LGM_{PMIP3} versus PI. Herein, the difference between LGM and PI is referred to as the ice-age effect. Due to the ice-age effect, the upper stratosphere in the LGM warms by up to 8 K, mainly because of much lower greenhouse gas concentrations and hence reduced radiative cooling to space. The reduced stratospheric warming in the NH high latitudes

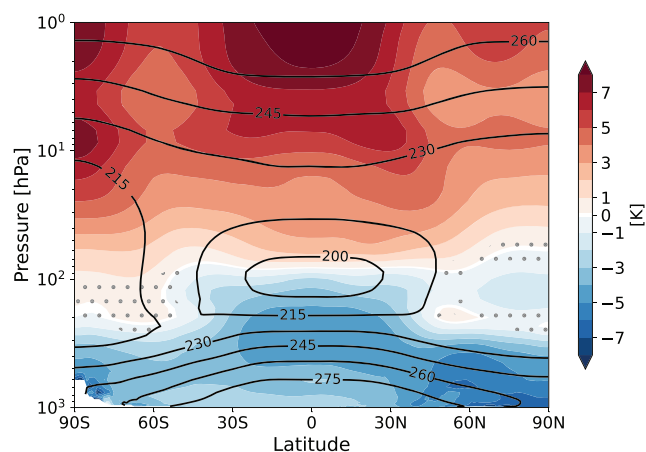


Figure 1. Annual mean zonal mean temperature change (color scale) for LGM_{PMIP3} versus PI. Black contours show the annual mean climatology (K) of PI. Regions that are not stippled are statistically significant at 95% confidence level, according to the Student's *t* test.

relative to the SH (Figure 1) reflects a dynamical cooling that is related to a weaker resolved wave drag in the NH high-latitude stratosphere and is consistent with a stronger zonal wind there (see Figure 5 in Fu et al., 2020). Such temperature changes agree with previous studies (Rind et al., 2001, 2009) and have a significant impact on stratospheric ozone concentration in the LGM, as will be shown later. The temperature changes in the troposphere are largely a response to the changes of SST, showing a maximum cooling of more than 4 K in the tropical upper troposphere as well as a cooling of up to 6 K in the NH high latitudes. Enhanced cooling is also seen over Antarctica. The global mean surface air temperature is 10.0°C in LGM_{PMIP3} and 10.5°C in LGM_{PROXY}, close to the “warm” LGM (10.7°C) of Murray et al. (2014) which was based on the SST reconstruction from CLIMAP (CLIMAP, 1976). The temperature changes in LGM_{PROXY} relative to PI are quite similar to LGM_{PMIP3} and thus not shown here.

3.2. Water Vapor and Hydroxyl Radical (OH) Changes

Water vapor transported from the tropical troposphere and oxidation of CH₄ in the stratosphere are the two primary sources of water vapor in the stratosphere (e.g., LeTexier et al., 1988). Water vapor transported upward across the tropical tropopause is largely determined by the tropopause temperatures (e.g., Randel et al., 2004). Based on in situ trace gas measurements, Pan et al. (2018) illustrated that the World Meteorological Organization lapse rate tropopause (LRT) (World Meteorological Organization, 1957) did better than the cold-point tropopause in identifying the transition from the troposphere to the stratosphere. Therefore, the LRT, namely, the lower boundary of a layer in which the temperature lapse rate is less than 2 K km^{−1} for a depth of at least 2 km, is used here.

Figure 2 shows the annual and zonal mean LRT temperature, water vapor concentration, and pressure versus latitude from the three simulations (left panels) and the corresponding changes relative to the PI (right panels). As compared to the PI, the ice-age conditions induce a cooling of ~1.5 K in the LRT in the tropics and NH high latitudes and 0.5 K cooling at the SH high latitudes (Figure 2b). It is also interesting to notice decreased cooling between about 35–65° latitudes in both hemispheres, which may be due to the equatorward shift of subtropical jets in cold climate (Fu et al., 2006; Fu & Lin, 2011). Relative to PI, the water vapor concentration at the LRT in the LGM is decreased by ~1 ppmv in the tropics and up to 3–6 ppmv at high latitudes (Figure 2d). The LRT pressure in the LGM is increased by ~5 hPa over the tropics and 10–20 hPa over the extratropics, as compared to the PI (Figure 2f). The changes in temperatures, water vapor, and pressure at the LRT are very similar to those at the cold point tropopause over the tropics (not shown).

The relative changes of stratospheric water vapor, excited atomic oxygen (O(¹D)), OH, and NO_x for LGM_{PMIP3} versus PI are shown in Figure 3, in which the climatology of PI is superimposed as contours in ppmv, ppqv, pptv, and ppbv, respectively. Stratospheric water vapor mixing ratio tends to increase with height because of increasing CH₄ oxidation (LeTexier et al., 1988). There is a local minimum of water vapor concentration at the South Pole owing to extreme cold temperatures there and associated dehydration through cloud particle sedimentation. Relative to PI, stratospheric water vapor in the LGM is decreased everywhere, with a 10–25% decrease in the lower and middle stratosphere and an ~20% decrease in the upper stratosphere, as a consequence of much lower atmospheric CH₄ concentrations (Table 1), and the colder tropical LRT (Figure 2b) leading to less water vapor transported from the troposphere (Figure 2d). O(¹D) is decreased above 2 hPa but increased by 5–15% in most other regions (Figure 3b), which is largely governed by the change in UV. OH is mainly produced by the reaction of O(¹D) with water vapor. In line with the decrease in stratospheric water vapor, stratospheric OH is decreased by 10–20% over the bulk of the stratosphere during the LGM (Figure 3c), despite the increase of O(¹D) below 2 hPa (Figure 3b). The reaction of N₂O with O(¹D) is the major source of stratospheric NO_x. Because of much higher UV radiation at higher altitudes, the climatological NO_x concentrations tend to increase with height, maximizing around 2 hPa (Figure 3d). Due to the much lower N₂O concentration in the LGM, the NO_x mixing ratio is decreased by 10–20% in the stratosphere, with small but significant increases around the NH high latitudes at ~100 hPa. The detailed pattern of NO_x changes (Figure 3d) is again determined by the changes of both N₂O and O(¹D), and the small increases of NO_x concentrations around the NH high latitudes near 100 hPa may be due to increases of O(¹D) there (Figure 3b).

Compared with LGM_{PMIP3}, more water vapor is transported from the troposphere into the stratosphere in LGM_{PROXY} because of the warmer tropical SST. Both stratospheric water vapor and OH in LGM_{PROXY} are

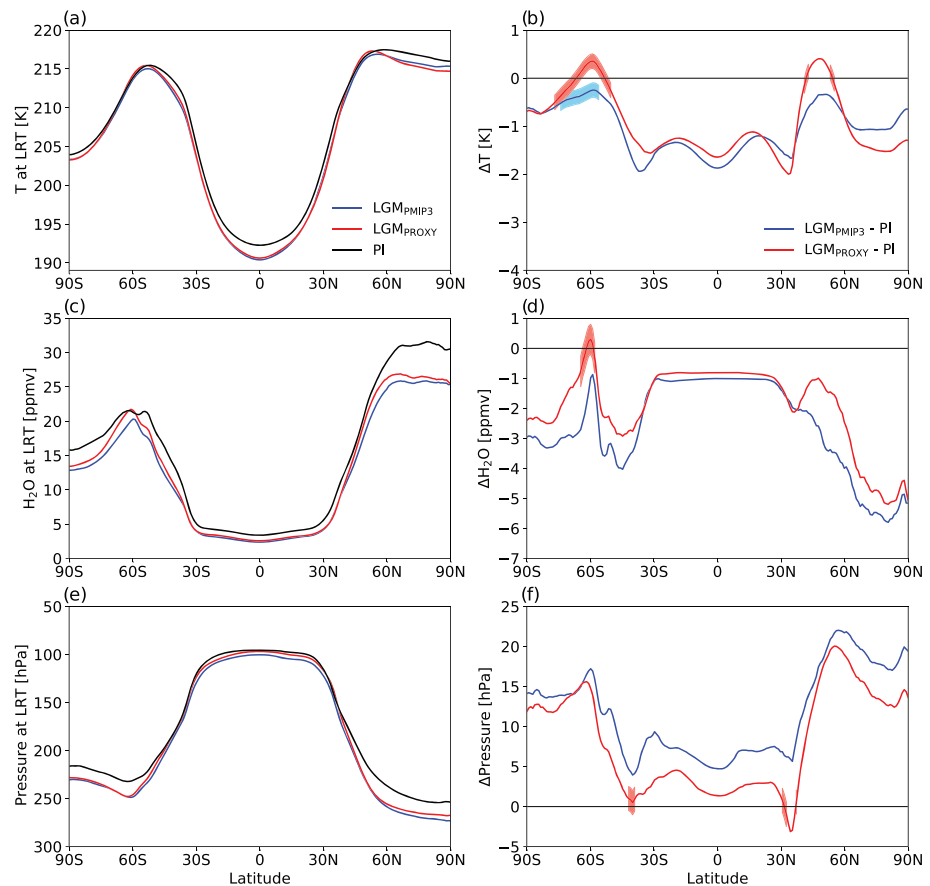


Figure 2. Annual mean zonal mean (a) lapse rate tropopause (LRT) temperature, (c) LRT water vapor (H_2O) concentration, and (e) LRT pressure in three simulations. Panels (b)–(f) are the corresponding changes relative to PI. Lines in panels (b)–(f) that are not shaded are statistically significant at 95% confidence level, according to the Student's t test.

thus a bit higher than LGM_{PMP3}, but the changes relative to PI remain similar (not shown). For brevity, unless otherwise indicated, the results of LGM_{PROXY} are not shown in the following discussions.

3.3. Ozone Change

Figure 4 shows the ozone change for LGM_{PMP3} versus PI. Relative to the PI, ice-age conditions lead to ozone decreases in most of the stratosphere but with a few exceptions. In the tropical lower stratosphere, the ozone is increased by 5–15%, extending up to about 20 hPa. The increase of ~5% near 10 hPa is caused by the

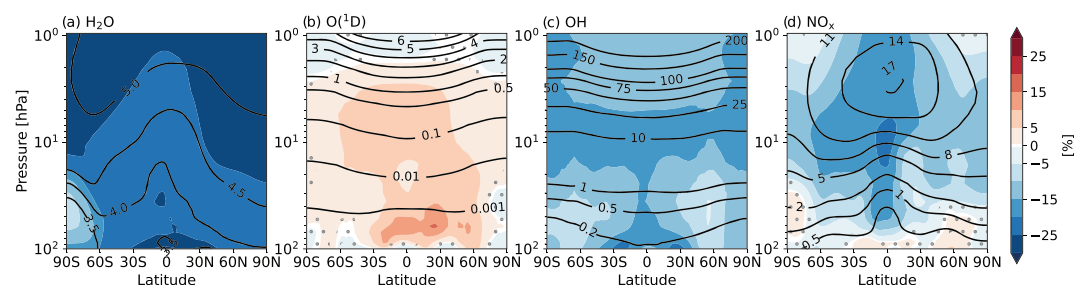


Figure 3. Annual mean zonal mean percentage changes (color scale) of (a) water vapor (H_2O), (b) excited atomic oxygen $\text{O}(^1\text{D})$, (c) hydroxyl radical (OH), and (d) nitrogen oxides (NO_x) for LGM_{PMP3} versus PI. Black contours show the climatology of PI expressed in (a) ppmv, (b) ppqv, (c) pptv, and (d) ppbv. Regions that are not stippled are statistically significant at 95% confidence level, according to the Student's t test.

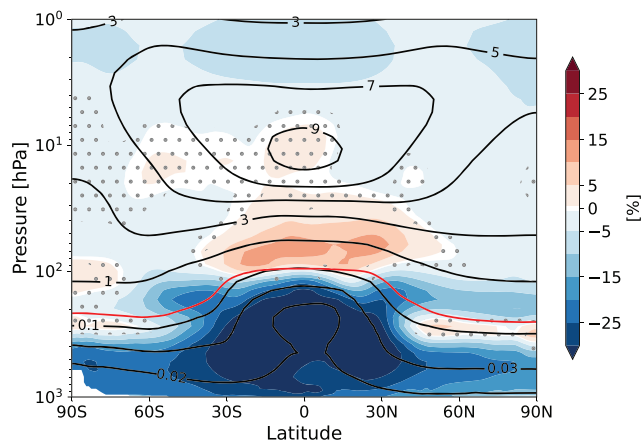


Figure 4. Annual mean zonal mean percentage change of ozone (color scale) for LGM_{PMIP3} versus PI. Black contours show the climatology (ppmv) of PI, and the red line represents the lapse rate tropopause of the PI. Regions that are not stippled are statistically significant at 95% confidence level, according to the Student's *t* test.

maximum reductions in OH and NO_x there (Figure 3), while the increase around 100 hPa over the SH high latitudes is linked to the local intensification of BDC in the spring season (see Figure 3e in Fu et al., 2020). The increases near ~300 hPa in both NH and SH extratropics are caused by lower tropopauses in the LGM which will be discussed later. The increase in tropical lower stratospheric ozone is due to a decrease in the BDC in the LGM (Fu et al., 2020) and will be further discussed later. Compared to PI, major catalysts of stratospheric ozone destruction including both OH and NO_x are decreased in the LGM (Figure 3), which will act to decrease stratospheric ozone loss rates. On the other hand, owing to the reduced greenhouse gas concentrations, the stratosphere warms by up to 8 K in the LGM (Figure 1). It is well known that stratospheric ozone in the upper stratosphere has an inverse relationship with temperature linked to gas-phase kinetic factors for several important ozone destruction reactions displaying a positive and large energy of activation (Chiodo et al., 2018; Haigh & Pyle, 1982; Jonsson et al., 2004). For example, as shown in Jonsson et al. (2004), in response to doubled CO₂-induced stratospheric cooling, stratospheric ozone increases because of the nonlinear changes in the reaction rate constants with changing temperature which especially slow the Chapman reaction $O + O_3 \rightarrow 2O_2$ and thus slow ozone destruction

rates. A warmer LGM stratosphere, on the other hand, leads to somewhat faster ozone loss reaction rates due to the temperature-sensitive reactions, which act to lower ozone concentrations. The net result of these compensating effects is only a 5–10% decrease in upper stratospheric ozone despite large changes in stratospheric temperatures, generally consistent with previous LGM studies (Crutzen & Brühl, 1993; Martinerie et al., 1995).

Unlike the upper stratosphere, in which ozone photochemistry dominates, the BDC plays a significant role in determining the lower stratospheric ozone distribution (Brasseur & Solomon, 2006; Li et al., 2009).

Following Li et al. (2009), the mean advective ozone transport $-\left(\overline{w^*} \frac{\partial \overline{O_3}}{\partial z} + \overline{v^*} \frac{\partial \overline{O_3}}{\partial y}\right)$ in the model is presented in Figure 5. Here, $\overline{w^*}$ and $\overline{v^*}$ are the transformed Eulerian mean (TEM) residual vertical and meridional velocity (Andrews et al., 1987), and $\overline{O_3}$ is the zonal mean ozone mixing ratio. The vertical $(-\overline{w^*} \frac{\partial \overline{O_3}}{\partial z})$ and meridional $(-\overline{v^*} \frac{\partial \overline{O_3}}{\partial y})$ components of advective ozone transport are also shown (middle and far right panels

of Figure 5). Note that we do not consider the role, if any, of quasi-horizontal mixing here, which is difficult to diagnose in chemistry-climate models because of the lack of the general theory behind it (Holton et al., 1995; Plumb, 2002). In the lower stratosphere (below ~15 hPa), the advective ozone transport is negative in the tropics but positive in the extratropics. By contrast, there is positive (negative) advective ozone transport in the tropics (extratropics) in the upper stratosphere. Generally, the advective ozone transport pattern is dominated by the vertical component because of much larger ozone vertical gradients compared to those in the horizontal (see contours of Figure 4). It is interesting to note that meridional ozone transport tends to increase ozone everywhere, except in the subtropical jet regions around the tropopause. The vertical and meridional advective ozone transport are stronger in the NH than the SH, reflecting the stronger BDC there (Rosenlof, 1995).

Fu et al. (2020) found that the BDC in the LGM is slower than that in the modern climate, regardless of SSTs prescribed. Consistent with the weakening BDC in the LGM, the change of advective ozone transport (Figures 5d–5f) is similar to, but generally the reverse sign of, the climatological pattern (Figures 5a–5c). The positive change of ozone advective transport in the tropical lower stratosphere (Figure 5d) explains the increase of ozone there in the LGM as already noted above (Figure 4). The ozone advective lifetime is much longer than the chemical loss lifetime in the upper stratosphere (Li et al., 2009). Hence, although LGM changes in advective ozone transport act to increase ozone in the upper stratosphere in the middle and high latitudes, chemical processes dominate in this region, resulting in ozone decreases there.

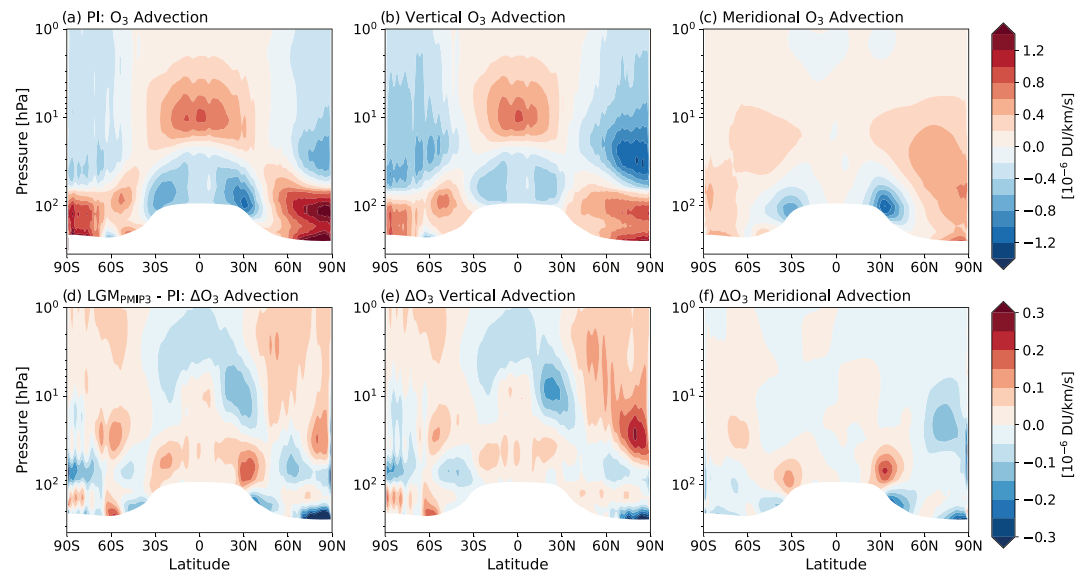


Figure 5. Advective ozone transport (far left), and its vertical (middle) and meridional (far right) components in the climatology of PI (a–c) and the changes in LGM_{PMP3} versus PI (d–f).

In order to further quantify the changes of ozone in the LGM, the total ozone column is divided into three parts: the upper stratospheric column (above 15 hPa) where chemical processes dominate, the lower stratospheric column (below 15 hPa but above the LRT) where dynamical transport dominates, and the tropospheric column (below the LRT). Figure 6 shows the annual and zonal mean latitudinal distributions of various ozone columns (upper panels) and their changes relative to the PI (lower panels). Since the lifetime of ozone related to chemical processes is much shorter than the time scale of advective transport in the upper stratosphere and the rate of ozone production is larger when the solar zenith angle is smaller (Brasseur & Solomon, 2006), the upper stratospheric ozone column peaks in the tropics and decreases toward the high latitudes (Figure 6a). In contrast, the lower stratospheric ozone column (Figure 6b) maximizes in the high latitudes, with a minimum at the tropics, mainly because of advective ozone transport. As expected, most of the ozone resides in the stratosphere (Figure 6c), and tropospheric ozone (Figure 6d) is only a small proportion (~10%) of the total ozone column. The tropospheric ozone has higher concentrations in midlatitudes

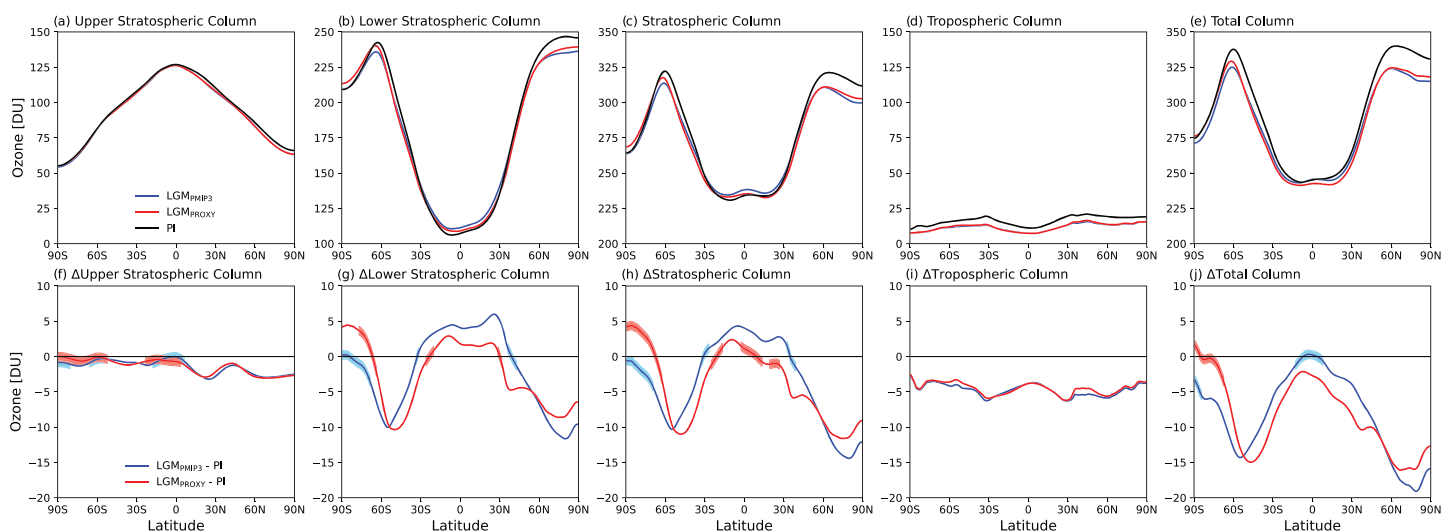


Figure 6. Annual mean zonal mean ozone column concentrations for various atmospheric layers (a–e) and the corresponding changes relative to PI (f–j). Lines in panels (f)–(j) that are not shaded are statistically significant at 95% confidence level, according to the Student's *t* test.

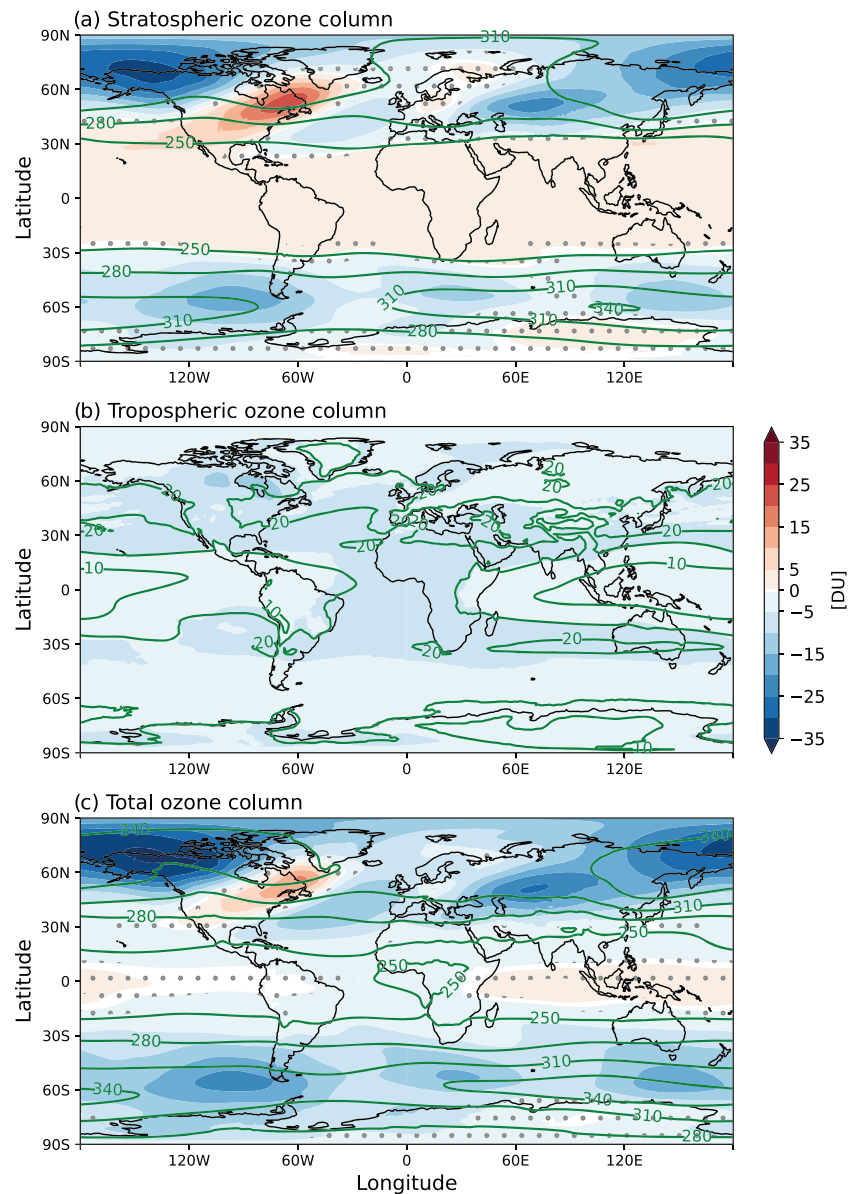


Figure 7. Spatial distribution of the changes (color scale) in the (a) stratospheric, (b) tropospheric, and (c) total ozone columns for LGM_{PMIP3} versus PI. The contours show the climatology of the PI. Regions that are not stippled are statistically significant at 95% confidence level, according to the Student's *t* test.

and higher concentrations in the NH than the SH. The latter results from higher photochemical ozone production related to higher natural continental emissions of CO, NO_x and hydrocarbons in the NH relative to the SH (e.g., Lelieveld & Dentener, 2000; Logan, 1985).

Due to the compensating effects of changes in major catalysts of ozone destruction (OH and NO_x) and temperature, ice-age conditions lead to a small (~1–3 DU) decrease of the upper stratospheric ozone column relative to PI (Figure 6f). Because of the weakening BDC, the lower stratospheric ozone column is increased by about 2–5 DU in the tropics and decreased by 5–10 DU in the extratropics (Figure 6g). The modeled change in the total stratospheric ozone column (Figure 6h) is dominated by change in the lower stratospheric ozone column (Figure 6g), agreeing with Chiodo et al. (2018), who investigated the response of ozone to quadrupled CO₂ concentrations. A reduced decrease (an increase) of lower-stratospheric ozone (Figure 6g) in the NH (SH) high latitudes is partly because of a lower tropopause there in the LGM as shown later.

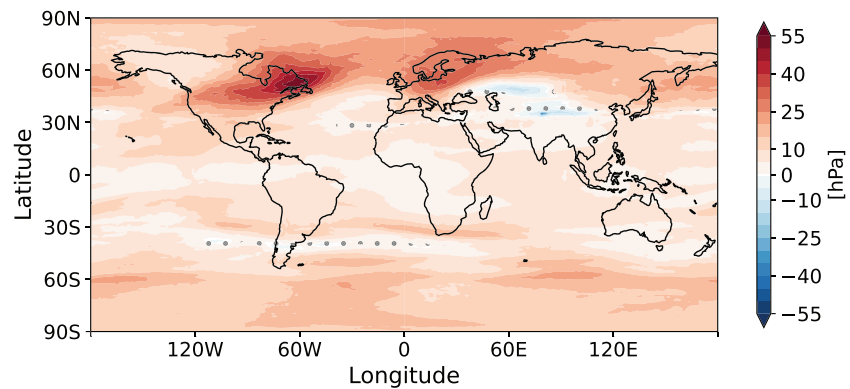


Figure 8. Spatial distribution of the changes in lapse rate tropopause pressure for LGM_{PMI3} versus PI. Regions that are not stippled are statistically significant at 95% confidence level, according to the Student's *t* test.

As compared with PI, the tropospheric ozone column is decreased by ~5 DU (30%) in the LGM (Figure 6i), which is at the upper end of the range ($-20 \pm 9\%$) given by Murray et al. (2014). The ice-age conditions lead to decreases (5–15 DU) of total ozone column at almost all latitudes except over SH high latitudes and deep tropics (Figure 6j). The latitudinal dependence of the total ozone column change is dominated by the lower stratospheric ozone column change (Figure 6g), while the tropospheric change shifts the total change down

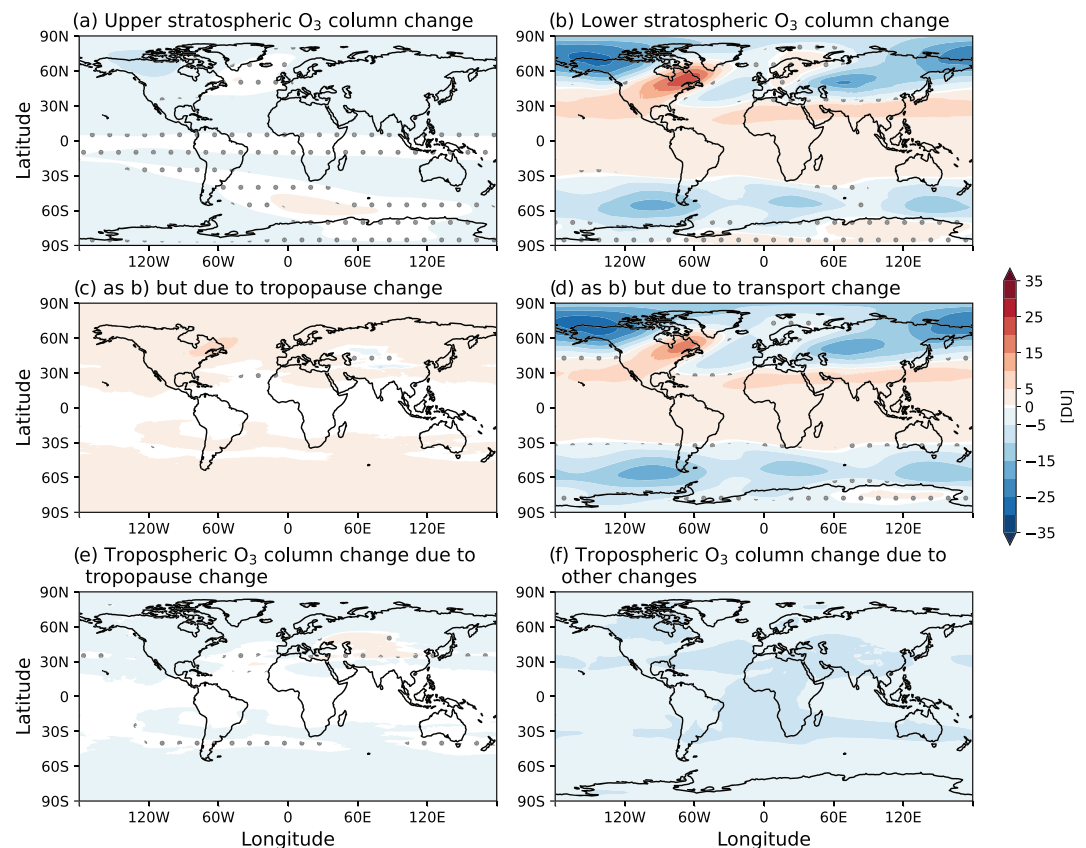


Figure 9. Spatial distribution of the changes in ozone column for LGM_{PMI3} versus PI. Panels (a) and (b) are the changes in the upper and lower stratospheric ozone columns, respectively. Panels (c) and (d) are the changes in the lower stratospheric ozone column due to the tropopause and transport changes, respectively. Panels (e) and (f) are the changes in the tropospheric ozone column due to the tropopause and other changes, respectively. Regions that are not stippled are statistically significant at 95% confidence level, according to the Student's *t* test.

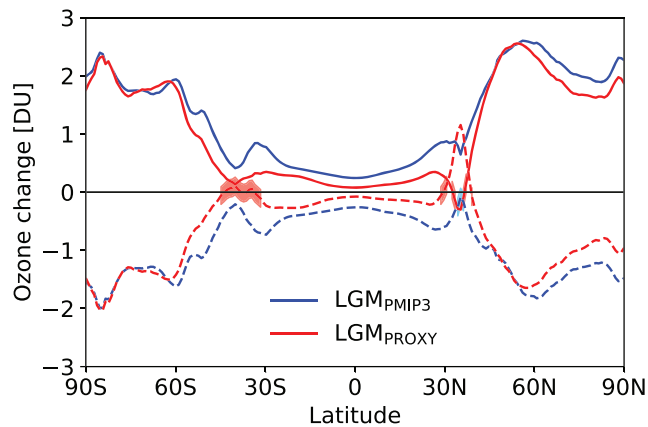


Figure 10. Annual mean zonal mean stratospheric (solid lines) and tropospheric (dash lines) ozone column changes due to the tropopause changes in the LGM_{PMIP3} (blue lines) and LGM_{PROXY} (red lines) versus PI. Lines that are not shaded are statistically significant at 95% confidence level, according to the Student's *t* test.

(Figure 8) and a strong local intensification of downward vertical motion (not shown). Those changes are probably driven by the presence of the Laurentide ice sheet and will further be investigated in the future.

Figures 9a–9d show the spatial distributions of upper and lower stratospheric ozone column changes for LGM_{PMIP3} versus PI and the contributions to the latter from the tropopause change and transport change. We quantify the lower stratospheric ozone column changes due to the tropopause change by integrating the LGM stratospheric ozone field vertically between LGM and PI tropopauses. By subtracting the contribution of tropopause change from the lower stratospheric ozone column change, the residual is referred to as the transport contribution. Consistent with Figure 6, the stratospheric ozone column change in the LGM (Figure 7a) is dominated by the lower stratospheric ozone change (Figure 9b). Further, we note that the contribution from tropopause changes leads to an increase of stratospheric ozone column in the extratropics (Figure 9c), which can also be seen in Figure 4 near 300 hPa. Although these changes are generally much smaller than those from transport changes (Figure 9d), they do partly compensate for the ozone decreases due to the circulation changes in the extratropics, especially in the SH (Figures 9 and 6).

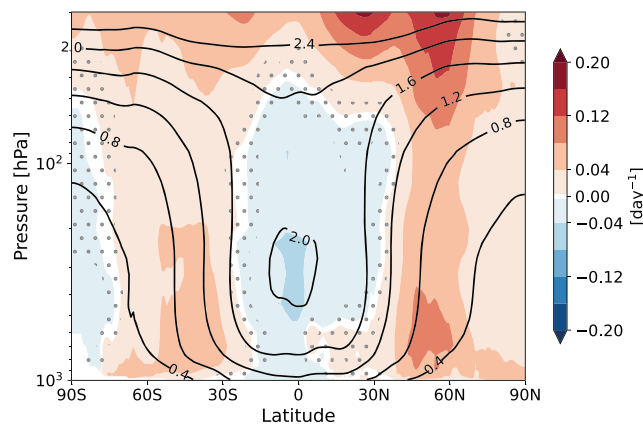


Figure 11. Annual mean zonal mean absolute change (color scale) in photolysis rate constant (J_{O1D}) for the reaction $O_3 + hv \rightarrow O_2 + O(^1D)$ in LGM_{PMIP3} versus PI. Black contours show the climatology (day^{-1}) of PI. Regions that are not stippled are statistically significant at 95% confidence level, according to the Student's *t* test.

by about 5 DU. Near the equator and South Pole the stratospheric and tropospheric ozone column changes tend to cancel each other.

Figure 7 shows the spatial distribution of stratospheric, tropospheric, and total ozone columns in the PI and the corresponding changes for LGM versus PI. As compared with PI, stratospheric ozone is increased slightly in the tropics but decreased by up to 25 DU in the NH middle and high latitudes (Figure 7a). Such a pattern of stratospheric ozone column change is similar to Murray et al. (2014), but with a smaller increase in the tropics (cf. our Figure 7a to their Figure 11). The larger decrease of the stratospheric ozone column in the NH relative to the SH is due to the larger magnitude decrease of the BDC in the NH (Fu et al., 2020). It is interesting to note that a large increase (~ 25 DU) of the stratospheric ozone column is found in northeast North America; this signal is statistically significant, regardless of SSTs prescribed. Murray et al. (2014) also found a large local increase (up to 30 DU) of stratospheric ozone column in the NH extratropics, but over Greenland, and only in their “warm” LGM simulation (see their Figure 11). It deserves to be mentioned that the large increase of stratospheric ozone column over northeast North America is collocated with the maximum LRT pressure increase

Relative to the PI, the tropospheric ozone column in the LGM is decreased everywhere, maximized around North America (Figure 7b), which may be due to the decrease of biogenic emissions and much higher tropospheric photolysis (Figures 13b and 13c) caused by the ice sheets. Here, the tropospheric ozone change for the LGM versus PI is consistent with theoretical expectation based on temperature-dependent surface emission of ozone precursor gases and does not support the hypothesis of Geng et al. (2017) that the transport of stratospheric ozone to the surface, driven by a stronger BDC, is increased in the glacial climate.

The tropospheric ozone column changes are caused by changes in in situ ozone formation, stratosphere-troposphere ozone exchange, and tropopause pressure. Higher tropopause pressures (i.e., lower tropopause altitudes) in the LGM (Figure 2f) would reduce the tropospheric ozone column concentration. We quantify this reduction as the ozone column concentration between the LGM and PI tropopauses with the PI ozone field. By subtracting the tropospheric ozone column change due to tropopause change, the residual is referred to as the contribution due to other changes associated with in situ formed ozone and stratosphere-troposphere ozone exchange. The lower tropopause in the LGM leads to the decreases of tropospheric ozone almost everywhere in middle and

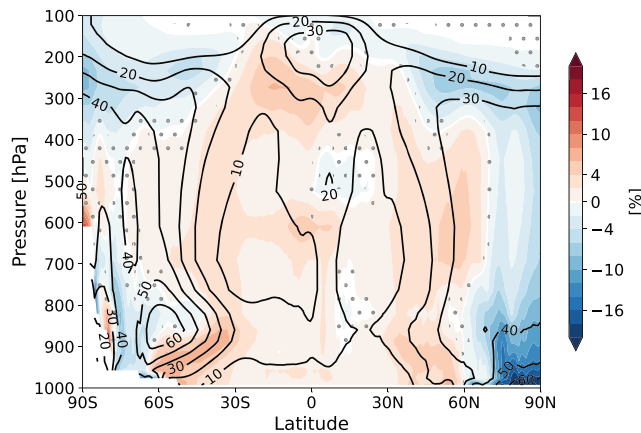


Figure 12. Annual mean zonal mean cloud fraction change (color scale) for LGM_{PMI3} versus PI. Black contours show the annual mean climatology (%) of PI. Regions that are not stippled are statistically significant at 95% confidence level, according to the Student's *t* test.

high latitudes (Figure 9e), but they are generally smaller than the contribution from other changes (Figure 9f). For the global mean, the lower tropopause results in a decrease of 0.7 (0.42) DU in the LGM_{PMI3} (LGM_{PROXY}) as compared with PI, which is 14.5% (9%) of the total tropospheric ozone decrease. Figure 10 shows the latitudinal dependence of the stratospheric and tropospheric ozone column changes due to the tropopause changes in the LGM_{PMI3} and LGM_{PROXY} versus PI. Consistent with Figure 9, the lower tropopause in the LGM leads to an increase (decrease) of stratospheric (tropospheric) ozone columns, with an impact of 1–3 DU (1–2 DU) over the extratropics.

The total ozone column in the LGM is decreased almost everywhere as compared to PI (Figure 7c), except at the northeast North America, equatorial Indian and West Pacific Oceans, because of larger stratospheric ozone increases (Figure 7a) relative to the tropospheric ozone decreases (Figure 7b) in those regions. In addition, only the increases over the northeast North America are statistically significant. It should be noted that the effect of tropopause change on the total ozone column is small since its effects on the stratospheric and tropospheric ozone columns are largely canceled each other (Figure 10).

3.4. UV Radiation Change

Ozone is one of the major factors determining surface UV radiation (Hall et al., 2018; Lamy et al., 2019), which in turn drives photochemical reactions in the troposphere. In this subsection, we investigate the change of photolytic rate constant (J_{O1D}) of $O_3 + h\nu \rightarrow O_2 + O(^1D)$, which is driven by photons at wavelengths shorter than 320 nm. The readers are referred to Madronich (1987) for the method used to calculate the photolytic rate constant that depends on atmospheric optical depth, surface albedo, and cloud fraction, as well as the overhead ozone column (Hall et al., 2018; Lamy et al., 2019). Figure 11 shows the annual and zonal mean J_{O1D} (day^{-1}) change for LGM versus PI. Because of the absorption of UV radiation by ozone, climatological J_{O1D} tends to decrease toward the surface, with the largest values in the tropics due to low ozone columns and small solar zenith angles. Compared to the PI, J_{O1D} in the LGM is decreased in the tropics and SH high latitudes, extending from 50 hPa toward the surface, but increased in other regions. The decrease of J_{O1D} for the LGM versus PI in the tropics is due to the increases of stratospheric ozone concentrations (Figure 4) and cloud fraction (Figure 12). For the SH high latitude, the decrease of J_{O1D} there is related to the increase in the stratospheric ozone column (Figure 4), while the increases in other regions are caused by the decreases in total ozone column abundance (Figure 7c). It is also noted that there are enhanced increases in J_{O1D} in the NH and SH midlatitudes near ~700 hPa.

Figure 13 shows the changes in the spatiotemporal distribution of surface J_{O1D} in the LGM. The seasonal cycle of surface J_{O1D} follows the seasonal progression of the solar zenith angle (Figure 13a). A maximum of surface J_{O1D} occurs over the Sahara Desert, which is related to the high surface albedo there. Higher J_{O1D} also occurs in regions with high topography, for example, Tibet and Andes, because of higher elevations and thus smaller solar attenuation by the atmosphere. In line with the change of total ozone column (Figure 7c), surface J_{O1D} in LGM is decreased in the tropics and the Antarctic but increased in most other regions, with the largest increase in North America and Europe in the boreal summer season caused by the increase in surface albedo and smaller solar attenuation resulting from the large ice sheets there (Figure 13b). A large increase of surface J_{O1D} is also found over the SH near 60°S, which is due to increased sea ice extent in the LGM. The relative change of surface J_{O1D} for LGM versus PI is shown in Figure 13c. It is interesting to note that, large relative changes (up to 100%) of the surface J_{O1D} exist in the NH high latitudes in the LGM, because of small climatological values there (see Figure 13a). The cloud fraction decreases in the high latitudes of the NH (Figure 12) may also make some contributions to the large increase of surface J_{O1D} there in the LGM, in addition to the total ozone column change (Figure 7c). On the other hand, an increase in clouds in the midlatitudes (Figure 12), especially in the SH, leads to a decrease in J_{O1D} there, partly compensating the effect of total ozone column change.

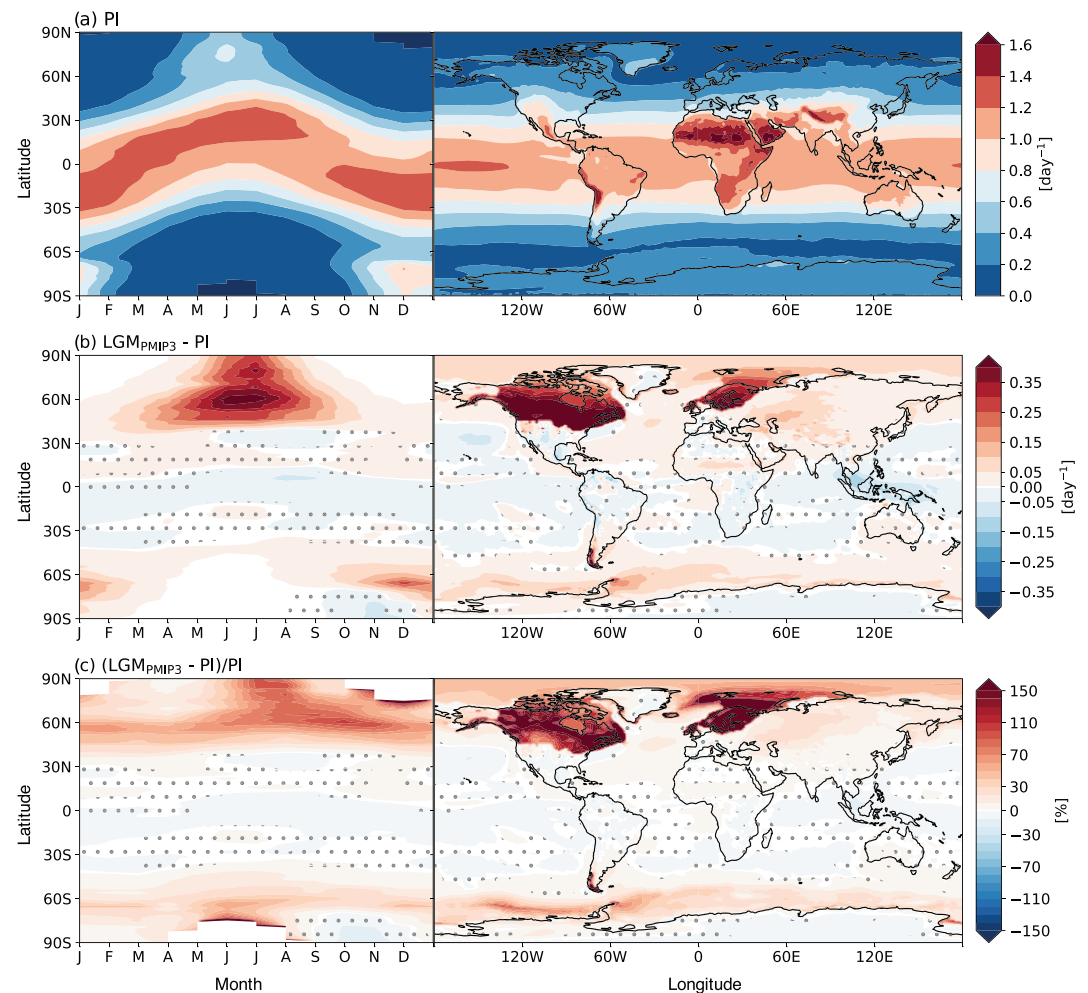


Figure 13. Spatiotemporal distribution of surface photolysis rate J_{O1D} in (a) PI simulation and (b) the absolute and (c) relative changes for LGM_{PMI3} versus PI. Each row contains two plots sharing a common ordinate axis (latitude). From left to right, a Hovmöller diagram presents the seasonality of zonal mean surface photolysis rate, and a map presents the horizontal distribution. Regions that are not stippled in (b) and (c) are statistically significant at 95% confidence level, according to the Student's t test.

Figure 13 indicates that the ice sheets have a large local impact on surface J_{O1D} change in the LGM. However, in regions not impacted by ice sheets (e.g., the tropics), the overhead ozone column abundance dominates the LGM change in J_{O1D} , resulting in decreases in photolysis rates in the tropics but increases in most other areas (Figures 11 and 13), as compared with the PI.

4. Conclusion and Discussion

We have investigated stratospheric ozone in the LGM using WACCM6. It is shown that, compared to the PI, water vapor in the LGM is decreased throughout the stratosphere, with an ~10–25% decrease in the lower and middle stratosphere and a 20% decrease in the upper stratosphere. This is largely owing to the much lower atmospheric CH_4 concentration, colder LRT (~1.5 K in the tropics), and less water vapor (~1 ppmv) at the LRT. In line with the lower stratospheric water vapor and N_2O concentrations in the LGM, stratospheric OH and NO_x are both decreased by 10–20%, which acts to decrease stratospheric ozone loss rates. On the other hand, because of the lower greenhouse gas concentrations, the stratospheric temperature is increased by up to 8 K in the LGM. This results in an increase in the ozone loss rate linked to temperature-sensitive gas-phase reactions, especially a faster Chapman reaction $O + O_3 \rightarrow 2O_2$ (Chiodo et al., 2018; Haigh & Pyle, 1982; Jonsson et al., 2004). The net result of these compensating effects is a

5–10% (1–3 DU) decrease in the upper stratospheric ozone concentration, generally consistent with previous studies (Crutzen & Brühl, 1993; Martinerie et al., 1995).

The BDC plays a significant role in determining the spatial distribution of ozone in the lower stratosphere. Contrary to Rind et al. (2001, 2009), who found a stronger BDC in the lowermost stratosphere in the LGM, Fu et al. (2020) showed that the BDC in the LGM is slower than the modern climate throughout the stratosphere, because of the decrease in the wave drags caused by the downward shift of the wave breaking associated with the zonal wind changes. Because of the weakening of the BDC in the LGM, lower stratospheric ozone is increased by 2–5 DU in the tropics and decreased by 5–10 DU in the extratropics. We also examined the effect of lower tropopause in the LGM, which increases the lower-stratospheric ozone in the extratropics by 1–3 DU and partly compensates the ozone decrease there due to the BDC changes.

In our simulations, we found that tropospheric ozone is decreased by about 5 DU (30%) in the LGM, as compared with the PI. Such a result is consistent with theoretical expectation based on temperature-dependent surface emissions of ozone precursor gases. The lower tropopause in the LGM makes a contribution to the decrease of the tropospheric ozone column by 1–2 DU in the extratropics. Murray et al. (2014) showed that transport of ozone from the stratosphere becomes an increasingly important fraction of the total tropospheric ozone in the cold climate, compared to the modern climate. Hence, changes in stratosphere-troposphere ozone exchange may play an important role in tropospheric chemistry in the LGM. The relative contributions of ozone formed in situ in the troposphere versus transport from the stratosphere in the LGM, and its implications for tropospheric chemistry, will be examined in a follow up paper.

It is interesting to note that stratospheric ozone is increased significantly in the northeast North America in the LGM, which is attributed to the local intensification of BDC induced by the Laurentide ice sheet. Compared to PI, the total ozone column in the LGM is decreased everywhere, except over the northeast North America, equatorial Indian and West Pacific Oceans, because of the larger stratospheric ozone increases relative to tropospheric ozone decreases there.

Compared to PI, surface J_{O1D} in the LGM is increased in most areas due to the decreased ozone column abundance. The largest increases are over North America and Europe because of the increase of surface albedo and smaller solar attenuation resulting from the large ice sheets. The large increase of surface J_{O1D} over the SH near 60°S is caused by the increased sea ice extent in the LGM. Surface J_{O1D} decreases in the tropics and the Antarctic in the LGM are due to the increases in the overhead ozone column abundance there. Such UV radiation change may have important ramifications for tropospheric chemistry (e.g., Murray et al., 2014), with potential implications for the methane lifetime as well as for interpretation of some paleoclimate records such as pollen (Benca et al., 2018). A dynamically consistent ozone field in the LGM can also be expected to be important for model simulations of the LGM climate (e.g., Chiodo & Polvani, 2017; Noda et al., 2017; Nowack et al., 2015; Szopa et al., 2019). Therefore, in addition to the implications for tropospheric chemistry, the ozone fields from this study are useful for the PMIP LGM climate simulations.

Acknowledgments

This research was supported by NSF Grant AGS-1821437 and NASA Grant 80NSSC18K1031. S. S. was supported by NSF AGS project 1848863. R. H. W. was partially funded by the European Union's Horizon 2020 research and innovation program under the Marie Skłodowska-Curie Grant Agreement No. 797961. We would like to acknowledge high-performance computing support from Cheyenne (doi:10.5065/D6RX99HX) provided by NCAR's Computational and Information Systems Laboratory, sponsored by the National Science Foundation, for the WACCM6 simulations and analyses presented in this study and for the data management, storage and preservation. The National Center for Atmospheric Research is sponsored by the United States National Science Foundation. We thank the anonymous reviewers for their constructive comments that have helped improve the manuscript.

Data Availability Statement

The data, including the ozone files which could be used in the model simulations of the glacial climate, can be obtained from the University of Washington Research Works Archive (through the link <http://hdl.handle.net/1773/45606>).

References

- Abe-Ouchi, A., Saito, F., Kageyama, M., Braconnot, P., Harrison, S. P., Lambeck, K., et al. (2015). Ice-sheet configuration in the CMIP5/PMIP3 Last Glacial Maximum experiments. *Geoscientific Model Development*, 8(11), 3621–3637. <https://doi.org/10.5194/gmd-8-3621-2015>
- Andrews, D. G., Leovy, C. B., & Holton, J. R. (1987). *Middle atmosphere dynamics*. New York: Academic Press.
- Benca, J., Duijnste, I. A. P., & Looy, C. V. (2018). UV-B induced forest sterility: Implications of ozone shield failure in Earth's largest extinction. *Science Advances*, 4, e1700618. <https://doi.org/10.1126/sciadv.1700618>
- Braconnot, P., Harrison, S. P., Kageyama, M., Bartlein, P. J., Masson-Delmotte, V., Abe-Ouchi, A., et al. (2012). Evaluation of climate models using palaeoclimatic data. *Nature Climate Change*, 2(6), 417–424. <https://doi.org/10.1038/nclimate1456>
- Brady, E. C., Otto-Bliesner, B. L., Kay, J. E., & Rosenbloom, N. (2013). Sensitivity to glacial forcing in the CCSM4. *Journal of Climate*, 26(6), 1901–1925. <https://doi.org/10.1175/jcli-d-11-00416.1>

- Brasseur, G. P., & Solomon, S. (2006). *Aeronomy of the middle atmosphere: chemistry and physics of the stratosphere and mesosphere*. New York: Springer Science & Business Media.
- Burkholder, J. B., Sander, S. P., Abbatt, J. P. D., Barker, J. R., Huie, R. E., Kolb, C. E., et al. (2015). Chemical kinetics and photochemical data for use in atmospheric studies: Evaluation number 18, Technical Report, Pasadena, CA: Jet Propulsion Laboratory, National Aeronautics and Space Administration, 2015.
- Chiodo, G., & Polvani, L. M. (2017). Reduced Southern Hemispheric circulation response to quadrupled CO₂ due to stratospheric ozone feedback. *Geophysical Research Letters*, 44, 465–474. <https://doi.org/10.1002/2016GL071011>
- Chiodo, G., Polvani, L. M., Marsh, D. R., Stenke, A., Ball, W., Rozanov, E., et al. (2018). The response of the ozone layer to quadrupled CO₂ concentrations. *Journal of Climate*, 31(10), 3893–3907. <https://doi.org/10.1175/JCLI-D-17-0492.1>
- CLIMAP (1976). The surface of the ice-age earth. *Science*, 191, 1131–1137. <https://doi.org/10.1126/science.191.4232.1131>
- Crutzen, P. J., & Brühl, C. (1993). A model study of atmospheric temperatures and the concentrations of ozone, hydroxyl, and some other photochemically active gases during the glacial, the preindustrial Holocene and the present. *Geophysical Research Letters*, 20(11), 1047–1050. <https://doi.org/10.1029/93GL01423>
- Emmons, L. K., Schwantes, R. H., Orlando, J. J., Tyndall, G., Kinnison, D., Lamarque, J. F., et al. (2020). The chemistry mechanism in the Community Earth System Model version 2 (CESM2). *Journal of Advances in Modeling Earth Systems*, 12, e2019MS001882. <https://doi.org/10.1029/2019MS001882>
- Fu, Q., Johanson, C. M., Wallace, J. M., & Reichler, T. (2006). Enhanced mid-latitude tropospheric warming in satellite measurements. *Science*, 312(5777), 1179–1179. <https://doi.org/10.1126/science.1125566>
- Fu, Q., & Lin, P. (2011). Poleward shift of subtropical jets inferred from satellite-observed lower-stratospheric temperatures. *Journal of Climate*, 24(21), 5597–5603. <https://doi.org/10.1175/jcli-d-11-00027.1>
- Fu, Q., White, R. H., Wang, M., Alexander, B., Solomon, S., Gettelman, A., et al. (2020). The Brewer-Dobson circulation during the Last Glacial Maximum. *Geophysical Research Letters*, 47, e2019GL086271. <https://doi.org/10.1029/2019GL086271>
- Garcia, R. R., & Richter, J. H. (2019). On the momentum budget of the quasi-biennial oscillation in the Whole Atmosphere Community Climate Model. *Journal of the Atmospheric Sciences*, 76(1), 69–87. <https://doi.org/10.1175/jas-d-18-0088.1>
- Geng, L., Murray, L. T., Mickley, L. J., Lin, P., Fu, Q., Schauer, A. J., & Alexander, B. (2017). Isotopic evidence of multiple controls on atmospheric oxidants over climate transitions. *Nature*, 546(7656), 133–136. <https://doi.org/10.1038/nature22340>
- Gettelman, A., Mills, M., Kinnison, D., Garcia, R., Smith, A., Marsh, D., et al. (2019). The Whole Atmosphere Community Climate Model Version 6 (WACCM6). *Journal of Geophysical Research: Atmospheres*, 124, 12,380–12,403. <https://doi.org/10.1029/2019JD030943>
- Guenther, A., Jiang, X., Heald, C., Sakulyanontvittaya, T., Duhl, T., Emmons, L., & Wang, X. (2012). The Model of Emissions of Gases and Aerosols from Nature version 2.1 (MEGAN2.1): An extended and updated framework for modeling biogenic emissions. *Geoscientific Model Development*, 5(6), 1471–1492. <https://doi.org/10.5194/gmd-5-1471-2012>
- Haigh, J., & Pyle, J. (1982). Ozone perturbation experiments in a two-dimensional circulation model. *Quarterly Journal of the Royal Meteorological Society*, 108(457), 551–574. <https://doi.org/10.1002/qj.49710845705>
- Hall, S. R., Ullmann, K., Prather, M. J., Flynn, C. M., Murray, L. T., Fiore, A. M., et al. (2018). Cloud impacts on photochemistry: Building a climatology of photolysis rates from the Atmospheric Tomography mission. *Atmospheric Chemistry and Physics*, 18(22), 16,809–16,828. <https://doi.org/10.5194/acp-18-16809-2018>
- Holton, J. R., Haynes, P. H., McIntyre, M. E., Douglass, A. R., Rood, R. B., & Pfister, L. (1995). Stratosphere-troposphere exchange. *Reviews of Geophysics*, 33(4), 403–439. <https://doi.org/10.1029/95RG02097>
- Jonsson, A. I., de Grandpre, J., Fomichev, V. I., McConnell, J. C., & Beagley, S. R. (2004). Doubled CO₂-induced cooling in the middle atmosphere: Photochemical analysis of the ozone radiative feedback. *Journal of Geophysical Research*, 109, D24103. <https://doi.org/10.1029/2004JD005093>
- Kaplan, J. O., Folberth, G., & Hauglustaine, D. A. (2006). Role of methane and biogenic volatile organic compound sources in late glacial and Holocene fluctuations of atmospheric methane concentrations. *Global Biogeochemical Cycles*, 20, GB2016. <https://doi.org/10.1029/2005GB002590>
- Kucera, M., Rosell-Mele, A., Schneider, R., Waelbroeck, C., & Weinelt, M. (2005). Multiproxy approach for the reconstruction of the glacial ocean surface (MARGO). *Quaternary Science Reviews*, 24(7–9), 813–819. <https://doi.org/10.1016/j.quascirev.2004.07.017>
- Lamy, K., Portafaix, T., Josse, B., Brogniez, C., Godin-Beekmann, S., Bencherif, H., et al. (2019). Clear-sky ultraviolet radiation modelling using output from the Chemistry Climate Model Initiative. *Atmospheric Chemistry and Physics*, 19(15), 10,087–10,110. <https://doi.org/10.5194/acp-19-10087-2019>
- Lelieveld, J., & Dentener, F. J. (2000). What controls tropospheric ozone? *Journal of Geophysical Research*, 105(D3), 3531–3551. <https://doi.org/10.1029/1999JD901011>
- LeTexier, H., Solomon, S., & Garcia, R. R. (1988). The role of molecular hydrogen and methane oxidation in the water vapour budget of the stratosphere. *Quarterly Journal of the Royal Meteorological Society*, 114(480), 281–295. <https://doi.org/10.1002/qj.49711448002>
- Levine, J. G., Wolff, E. W., Jones, A. E., & Sime, L. C. (2011). The role of atomic chlorine in glacial-interglacial changes in the carbon-13 content of atmospheric methane. *Geophysical Research Letters*, 38, L04801. <https://doi.org/10.1029/2010GL046122>
- Li, F., Stolarski, R. S., & Newman, P. A. (2009). Stratospheric ozone in the post-CFC era. *Atmospheric Chemistry and Physics*, 9(6), 2207–2213. <https://doi.org/10.5194/acp-9-2207-2009>
- Logan, J. A. (1985). Tropospheric ozone: Seasonal behavior, trends, and anthropogenic influence. *Journal of Geophysical Research*, 90(ND6), 10,463–10,482. <https://doi.org/10.1029/JD090iD06p10463>
- Madronich, S. (1987). Photodissociation in the atmosphere: 1. Actinic flux and the effects of ground reflections and clouds. *Journal of Geophysical Research*, 92(D8), 9740–9752. <https://doi.org/10.1029/JD092iD08p09740>
- Martinerie, P., Brasseur, G. P., & Granier, C. (1995). The chemical composition of ancient atmospheres: A model study constrained by ice core data. *Journal of Geophysical Research*, 100(D7), 14,291–14,304. <https://doi.org/10.1029/95JD00826>
- McLinden, C. A., Olsen, S. C., Hannegan, B., Wild, O., Prather, M. J., & Sundet, J. (2000). Stratospheric ozone in 3-D models: A simple chemistry and the cross-tropopause flux. *Journal of Geophysical Research*, 105(D11), 14,653–14,665. <https://doi.org/10.1029/2000JD900124>
- Murray, L. T., Mickley, L. J., Kaplan, J. O., Sofen, E. D., Pfeiffer, M., & Alexander, B. (2014). Factors controlling variability in the oxidative capacity of the troposphere since the Last Glacial Maximum. *Atmospheric Chemistry and Physics*, 14(7), 3589–3622. <https://doi.org/10.5194/acp-14-3589-2014>

- Noda, S., Kodera, K., Adachi, Y., Deushi, M., Kitoh, A., Mizuta, R., et al. (2017). Impact of interactive chemistry of stratospheric ozone on Southern Hemisphere paleoclimate simulation. *Journal of Geophysical Research: Atmospheres*, 122, 878–895. <https://doi.org/10.1002/2016JD025508>
- Noda, S., Kodera, K., Adachi, Y., Deushi, M., Kitoh, A., Mizuta, R., et al. (2018). Mitigation of global cooling by stratospheric chemistry feedbacks in a simulation of the Last Glacial Maximum. *Journal of Geophysical Research: Atmospheres*, 123, 9378–9390. <https://doi.org/10.1029/2017JD028017>
- Nowack, P. J., Abraham, N. L., Maycock, A. C., Braesicke, P., Gregory, J. M., Joshi, M. M., et al. (2015). A large ozone-circulation feedback and its implications for global warming assessments. *Nature Climate Change*, 5(1), 41–45. <https://doi.org/10.1038/nclimate2451>
- Oleson, K. W., Lawrence, D. M., Gordon, B., Flanner, M. G., Kluzek, E., Peter, J., et al. (2010). Technical description of Version 4.0 of the Community Land Model (CLM).
- Pan, L. L., Honomichl, S. B., Bui, T. V., Thornberry, T., Rollins, A., Hints, E., & Jensen, E. J. (2018). Lapserate or cold point: The tropical tropopause identified by in situ trace gas measurements. *Geophysical Research Letters*, 45, 10,756–10,763. <https://doi.org/10.1029/2018GL079573>
- Plumb, R. A. (2002). Stratospheric transport. *Journal of the Meteorological Society of Japan. Series II*, 80(4B), 793–809.
- Price, C., & Rind, D. (1992). A simple lightning parameterization for calculating global lightning distributions. *Journal of Geophysical Research*, 97(D9), 9919–9933. <https://doi.org/10.1029/92JD00719>
- Randel, W. J., Wu, F., Oltmans, S. J., Rosenlof, K., & Nedoluha, G. E. (2004). Interannual changes of stratospheric water vapor and correlations with tropical tropopause temperatures. *Journal of the Atmospheric Sciences*, 61(17), 2133–2148. [https://doi.org/10.1175/1520-0469\(2004\)061<2133:Icoswv>2.0.Co;2](https://doi.org/10.1175/1520-0469(2004)061<2133:Icoswv>2.0.Co;2)
- Rayner, N. A., Parker, D. E., Horton, E. B., Folland, C. K., Alexander, L. V., Rowell, D. P., et al. (2003). Global analyses of sea surface temperature, sea ice, and night marine air temperature since the late nineteenth century. *Journal of Geophysical Research*, 108(D14), 4407. <https://doi.org/10.1029/2002JD002670>
- Rind, D., Chandler, M., Loneragan, P., & Lerner, J. (2001). Climate change and the middle atmosphere 5. Paleostratosphere in cold and warm climates. *Journal of Geophysical Research*, 106(D17), 20,195–20,212. <https://doi.org/10.1029/2000JD900548>
- Rind, D., Lerner, J., McLinden, C., & Perlwitz, J. (2009). Stratospheric ozone during the Last Glacial Maximum. *Geophysical Research Letters*, 36, L09712. <https://doi.org/10.1029/2009GL037617>
- Rohrer, F., & Berresheim, H. (2006). Strong correlation between levels of tropospheric hydroxyl radicals and solar ultraviolet radiation. *Nature*, 442(7099), 184–187. <https://doi.org/10.1038/nature04924>
- Rosenlof, K. H. (1995). Seasonal cycle of the residual mean meridional circulation in the stratosphere. *Journal of Geophysical Research*, 100(D3), 5173–5191. <https://doi.org/10.1029/94JD03122>
- Solomon, S., Kinnison, D., Bandoro, J., & Garcia, R. (2015). Simulation of polar ozone depletion: An update. *Journal of Geophysical Research: Atmospheres*, 120, 7958–7974. <https://doi.org/10.1002/2015JD023365>
- Szopa, S., Thieblemont, R., Bekki, S., Botsyun, S., & Sepulchre, P. (2019). Role of the stratospheric chemistry-climate interactions in the hot climate conditions of the Eocene. *Climate of the Past*, 15(4), 1187–1203. <https://doi.org/10.5194/cp-15-1187-2019>
- Thornton, P. E., Lamarque, J. F., Rosenbloom, N. A., & Mahowald, N. M. (2007). Influence of carbon-nitrogen cycle coupling on land model response to CO₂ fertilization and climate variability. *Global Biogeochemical Cycles*, 21, GB4018. <https://doi.org/10.1029/2006GB002868>
- Valdes, P. J., Beerling, D. J., & Johnson, C. E. (2005). The ice age methane budget. *Geophysical Research Letters*, 32, L02704. <https://doi.org/10.1029/2004GL021004>
- Wegner, T., Kinnison, D. E., Garcia, R. R., & Solomon, S. (2013). Simulation of polar stratospheric clouds in the specified dynamics version of the whole atmosphere community climate model. *Journal of Geophysical Research: Atmospheres*, 118, 4991–5002. <https://doi.org/10.1002/jgrd.50415>
- World Meteorological Organization (1957). Meteorology—A three dimensional science: Second session of the Commission for Aerology. *WMO Bulletin*, IV(4), 134–138.